

Full Length Article



The mechanism for catalytic fast pyrolysis of levoglucosan, furfural and furan over HZSM-5: An experimental and theoretical investigation

Amin Osatiashtiani^{a,1,*}, Jiajun Zhang^{b,c,1}, Stylianos D. Stefanidis^{a,d}, Xiaolei Zhang^{c,*}, Anthony V. Bridgwater^a

^a Energy & Bioproducts Research Institute (EBRI), College of Engineering and Physical Sciences, Aston University, Aston Triangle, Birmingham B4 7ET, United Kingdom

^b Center for Combustion Energy, Key Laboratory for Thermal Science and Power Engineering of Ministry of Education, International Joint Laboratory on Low Carbon Clean Energy Innovation, Tsinghua University, Beijing 100084, China

^c Department of Chemical and Process Engineering, University of Strathclyde, Glasgow G1 1XJ, United Kingdom

^d Chemical Process and Energy Resources Institute, Centre for Research and Technology Hellas, Thessaloniki 57001, Greece

ARTICLE INFO

Keywords:

Catalytic fast pyrolysis
Zeolite
DFT modelling
Levoglucosan

ABSTRACT

In this work, we have investigated the complicated reaction network of biomass catalytic fast pyrolysis, particularly the decomposition of the key cellulose pyrolysis intermediate, levoglucosan. Fast pyrolysis of levoglucosan using a Py-GC-MS-FID system in the presence of HZSM-5 suggested that furan and furfural are key intermediates to aromatic hydrocarbons. This was followed by theoretical modelling adopting density functional theory (DFT) to unravel the details of the catalytic reaction mechanism from levoglucosan to furan. Our investigations revealed for the first time a direct route from levoglucosan to furan without furfural as an intermediate, with the highest energy barrier along the most favourable pathway to be 2.15 eV. Combined with previously reported mechanisms in the literature, we provide here a detailed reaction network for the conversion of cellulose-derived intermediates to aromatic hydrocarbons.

1. Introduction

In the quest for independence from fossil energy sources and mitigation of climate change, lignocellulosic biomass is considered a promising renewable feedstock for the production of biofuels and chemical products [1,2]. Lignocellulosic biomass can be converted directly to liquid, solid and gas products via fast pyrolysis. During fast pyrolysis, biomass is rapidly heated to temperatures around 450–550 °C under inert atmosphere and atmospheric pressure. Under these conditions, the structural biopolymers in biomass (cellulose, hemicellulose and lignin) are thermally decomposed and pyrolysis vapours are formed, which can be rapidly quenched to obtain a liquid product, known as bio-oil, with reported yields up to 60–75 % [3]. Bio-oil is a mixture of over 400 oxygenated compounds and oligomers [4,5] that are formed via a highly complex network of primary depolymerisation reactions, as well as secondary cracking and repolymerisation reactions of the volatiles in the vapour phase. Owing to its high oxygen and water content, bio-oil has a low calorific value, is immiscible with petroleum-derived fuels, corrosive and relatively unstable under heating, storage and

transportation conditions, hindering its direct application as a fuel [6].

A liquid product with improved properties can be obtained by incorporating a heterogeneous catalyst during fast pyrolysis, either *in situ* or *ex situ*, in a process known as catalytic fast pyrolysis. In the presence of a catalyst, the vapours released from biomass react on the surface of the catalyst and some oxygen is removed in the form of CO₂, CO and H₂O to produce partially deoxygenated compounds and hydrocarbons [7]. As a result, a less oxygenated liquid is obtained that is less corrosive and has improved calorific value and stability [8]. The physicochemical properties of the catalyst, such as its structural architecture, acidity, and the number of active sites have a significant impact on the deoxygenation pathway and the distribution of the catalytic pyrolysis products [9,10]. HZSM-5 is one of the most studied catalysts for biomass pyrolysis, owing to its acidity and unique shape selectivity that promotes the formation of desirable aromatic hydrocarbons and partially mitigates the formation of undesirable catalytic coke [11]. The catalytic product can serve as an intermediate that can be readily upgraded to transportation fuels or value-added chemicals via downstream processing [12–14]. Inevitably, the mass yield of liquid is

* Corresponding authors.

E-mail addresses: a.osatiashtiani@aston.ac.uk (A. Osatiashtiani), xiaolei.zhang@strath.ac.uk (X. Zhang).

¹ These authors contributed equally to this work.

reduced compared to non-catalytic pyrolysis due to the removal of oxygen, as well as undesirable reactions that lead to carbon loss via the formation of catalytic coke and permanent gases [15].

Understanding the underlying reaction mechanisms and tracking the pathways of oxygen rejection holds the key to rational catalyst design and to tuning catalytic fast pyrolysis selectivity towards desirable products [16]. However, this is a very challenging task, owing to the complex composition of the products released from biomass, which undergo numerous parallel and successive reactions during pyrolysis. The presence of a heterogeneous catalyst adds an additional layer of complexity to the reaction network during fast pyrolysis, since the intermediates that are formed from activated primary pyrolysis products are short-lived and challenging to determine experimentally [17]. To address this challenge, the combination of experimental studies using pyrolysis vapour model compounds with computational modelling based on density functional theory (DFT) has emerged as a reliable approach to investigate biomass catalytic fast pyrolysis mechanisms.

There are several reports on the overall reaction pathways of catalytic biomass pyrolysis [18–21]. In this regard, acidic zeolites such as HZSM-5 are evidenced to be effective catalysts for the fast pyrolysis of cellulose [20]. It is generally accepted that the catalytic fast pyrolysis of cellulose over HZSM-5 takes place through cellulose depolymerisation, levoglucosan formation, formation of furanic compounds, followed by dehydration and aromatisation. However, the mechanism of the catalytic decomposition of cellulose in the presence of heterogeneous catalysts in general, and HZSM-5 in particular, have rarely been explored at the atomic level.

Among all the products of biomass fast pyrolysis, levoglucosan (LG) has been identified as one of the major products of lignocellulosic biomass pyrolysis [22,23], which is known to be derived from the decomposition of cellulose via a *trans*-glycosylation mechanism [24–26]. Thus, understanding the LG reaction mechanism has received significant attention because it is considered a critical step to elucidate the biomass pyrolysis mechanism [27,28]. Huber et al. has proposed a detailed kinetic model of cellulose pyrolysis to LG [29]. Maliakkal et al. also investigated the transglycosylation mechanism during cellulose decomposition and proposed adjacent OH promotes C–O activation by stabilising the charged transition state and facilitating proton transfer [30].

Depending on the pyrolysis conditions such as residence time, reactor configuration, as well as the presence of a catalyst and its type, LG can undergo further secondary thermal and catalytic reactions, which can alter the product yields and distribution [31,32]. The mechanism of LG decomposition during cellulose fast pyrolysis is complicated and is a matter of debate. There has long been an awareness of a catalytic effect of alkali metals in biomass ash which affects the cracking of LG, but this is outside the scope of this paper. Shen et al. [25] experimentally investigated the product distribution from the non-catalytic secondary cracking of LG during the decomposition of cellulose in the temperature range of 430–730 °C. They concluded that LG undergoes hydrolysis before a ring opening reaction, and that LG acts as an intermediate for the formation of C₂ to C₄ products. In particular, pyruvaldehyde was found to be produced from LG decomposition at high temperatures. Zhang et al. employed DFT modelling to study the initial thermal decomposition of LG, and also concluded that dehydration is more favourable at the beginning of the reaction than C–O and C–C bond cracking [33]. Fang et al. proposed systematic decomposition pathways of glucose based on experimental work, indicating that apart from furfural and 5-hydroxymethylfurfural (HMF), 3-Hydroxy- γ -butyrolactone and 3-(2H)-furanone were also identified as products, and their formation mechanisms were investigated in detail by DFT modelling [34]. Furthermore, Seshadri et al. investigated the reactions taking place on glucose by DFT modelling, and provided mechanism insights towards the effects of adjacent hydroxy groups to the formation of LG, revealing the relationship between Brønsted acid strength to the intrinsic activation energy [35,36].

Despite numerous reports on the reaction mechanism of LG during non-catalytic pyrolysis [33,37–45], there is still lack of information regarding the exact conversion pathway of LG and its mechanism. In this work, the thermal (non-catalytic) and catalytic decomposition mechanisms of LG were investigated experimentally, and in combination with DFT calculations. Non-catalytic and catalytic pyrolysis of LG with a HZSM-5 zeolite was carried out using a Py-GC–MS-FID system at variable temperatures and catalyst-to-feed ratios in order to determine primary and secondary products from thermal and catalytic reactions. Based on the experimentally determined products, possible reaction mechanisms for the catalytic conversion of LG were proposed and evaluated with DFT calculations. The work was supplemented with thermal and catalytic pyrolysis experiments of furfural and furan, which were determined to be major products of the catalytic conversion of LG, and reaction mechanisms were proposed accordingly. Thus, this research aims to combine an experimental approach with theoretical modelling to provide sound insights into the decomposition of LG taking place over HZSM-5 during the biomass catalytic fast pyrolysis.

2. Materials and methods

2.1. Py-GC–MS-FID experimental setup

The product distribution of the thermal (non-catalytic) and catalytic fast pyrolysis of LG (1,6-Anhydro- β -D-glucose 99 %, Sigma-Aldrich), furan (≥ 99 %, Sigma-Aldrich) and furfural (99 %, Sigma-Aldrich) was investigated by Py-GC–MS-FID on a CDS (Chemical Data Systems, Oxford, PA) 5200 series pyrolyser, close-coupled to a PerkinElmer Clarus 680 gas chromatograph (GC), equipped with a flame ionisation detector (FID) and Clarus 600S mass spectrometer (MS). All experiments were conducted using 0.5 mg of the starting material which was placed inside a 25 mm quartz tube between quartz wool. Due to the low boiling point of furan (31.4 °C), it was practically impossible to accurately weight it out and conduct the tests at specific catalyst: feed ratios. Therefore, only a test with an approximate catalyst: feed ratio of 5 and a non-catalytic test were conducted. A ZSM-5 zeolite (Alfa Aesar, SiO₂/Al₂O₃ molar ratio = 84.7) was used for all the catalytic pyrolysis experiments. The catalyst was obtained in ammonium form and was calcined at 600 °C for 6 h in static air prior to the pyrolysis experiments to convert it to proton form. For the catalytic experiments, the catalyst was divided into two portions and each portion was placed on either side of the biomass feedstock and further fixed in place with quartz wool. As such, the feed and catalyst were separated with layers of quartz wool and the configuration resembled the *ex situ* catalytic fast pyrolysis, where the feedstock is not in direct contact with the catalyst.

For each experiment, the sample tube was placed inside a platinum coil probe, which was heated to the desired reaction temperature (500, 550 or 600 °C) at 20 °C ms⁻¹ heating rate, with a hold time of 30 s, under a He (20 ml min⁻¹) carrier gas flow. Volatilised compounds were immediately trapped on a Tenax ®-TA adsorbent trap at 45 °C to avoid secondary/recombination reactions. The interface between the probe and the trap was maintained at 350 °C to prevent vapour condensation. It is important to note that LG has a boiling point of 385 °C, so needs careful handling in a Pyroprobe. The Tenax ®-TA adsorbent trap was then heated to 295 °C and held at this temperature for 2 min to re-release the pyrolysis products, which were transferred to the GC column via a heated transfer line kept at 310 °C. The separation of the compounds was carried out using a PerkinElmer Elite-1701 column (cross-bond, 14 % cyanopropylphenyl and 85 % dimethyl polysiloxane; 30 m, 0.25 mm inner diameter, and 0.25 mm film thickness). The GC oven was held at 45 °C for 5 min, then heated at 5 °C min⁻¹ to 250 °C and held at this temperature for 5 min. The separated compounds were analysed by the MS and the FID. The compounds were identified by comparing the mass spectra obtained from the MS (*m/z* 45–300) to mass spectra in the NIST11 MS library. As a general rule, an arbitrary minimum similarity threshold of 70 % was employed. The peak areas of each compound

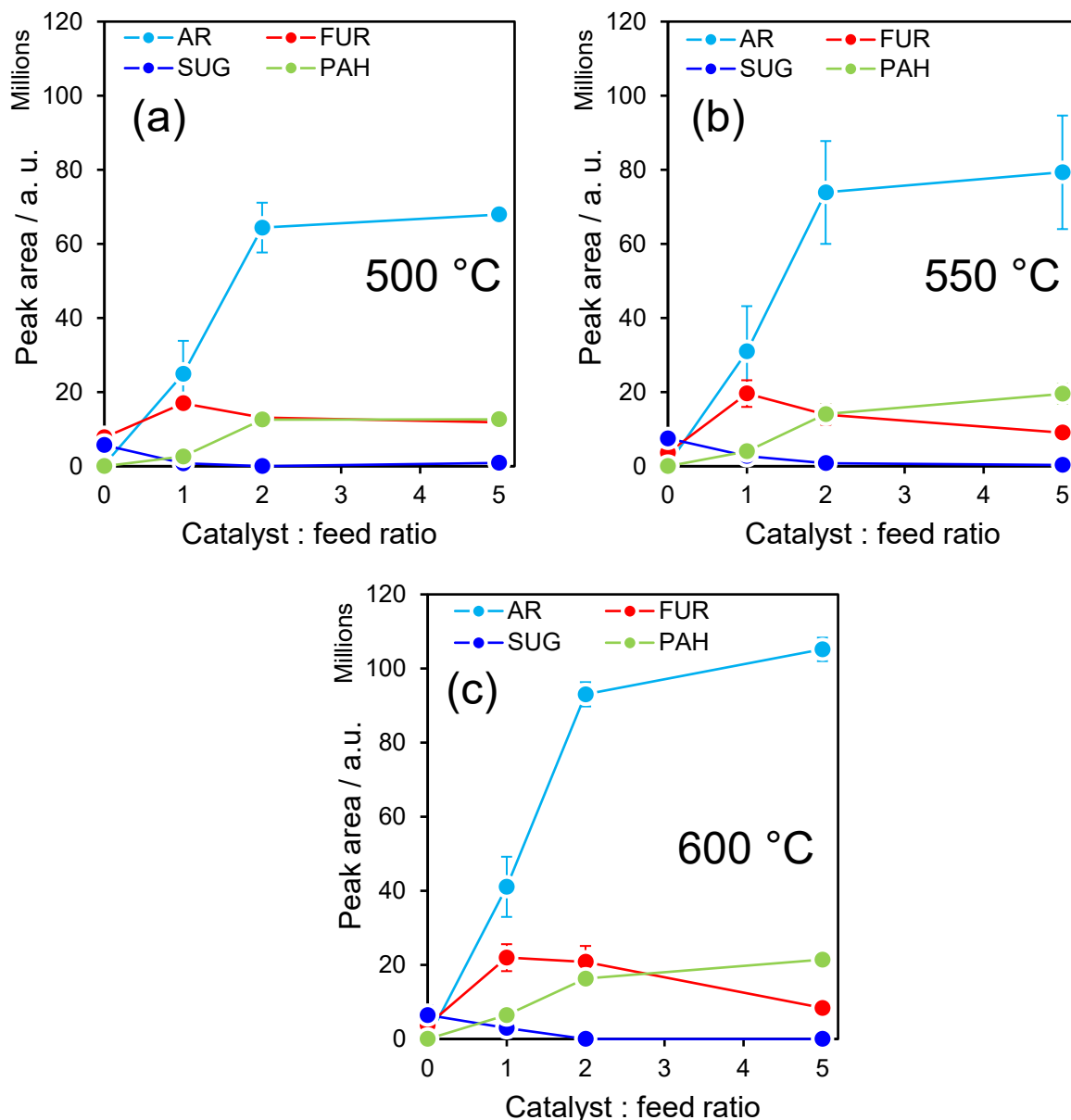


Fig. 1. Abundance of the main groups of products from LG thermal and catalytic fast pyrolysis at a) 500 °C, b) 550 °C and c) 600 °C.

were obtained from the FID chromatogram. All experiments were performed at least in duplicate to confirm the reproducibility of the reported procedure. The yield of the solid pyrolysis products (char, plus coke on catalyst) was quantified by combustion of the pyrolysed sample tubes in a muffle furnace at 700 °C for 15 min in static air. The sample tubes were weighed pre- and post-combustion using a Mettler Toledo microbalance (± 0.001 mg) and the yields of the solid products were calculated according to Eq. (1).

$$\text{Solid products \%} = \frac{t_i - t_f}{m_i} \times 100 \quad (1)$$

where t_i is the pre-combustion mass of the sample tube, t_f is the post-combustion mass of the tube, and m_i is the initial mass of the biomass feedstock that was pyrolysed.

2.2. Computational details

The first-principle DFT calculation was implemented in CASTEP (a leading code for calculating the properties of materials from first prin-

ciples) with dispersion correction, and the models were established in Materials Studio 2017 R2 [46,47]. The generalised gradient corrected approximation (GGA) treated by the Perdew – Burke – Ernzerhof (PBE) exchange–correlation potential with long-range dispersion correction via Grimme’s scheme was used to calculate the exchange–correlation energy [48,49]. The on-the-fly generated (OTFG) ultra-soft pseudopotential was employed as the scheme in the representation of reciprocal space for all the elements [50–52]. For this study, the plane-wave cut-off energy was set to 1000 eV for all the calculations based on the independence test (Fig. S1). The Brillouin zone was sampled using a $2 \times 2 \times 1$ Monkhorst-Pack k-point (spacing of 0.03 \AA^{-1}) with a smearing of 0.1 eV. The initial configuration of the catalyst was obtained from the siliceous ZSM-5 crystal, and an 8 T model was extracted to simulate the performance of a Brønsted acid site [53,54]. A 20 Å vacuum region was created above the top of the catalyst model, as shown in Fig. S2. The self-consistent field (SCF) tolerance was set to 10^{-6} eV/atom. The entire calculation was performed with a convergence threshold of 10^{-5} eV/atom on energy, 0.03 eV/Å on maximum force, and 10^{-3} Å on the maximum displacement. No symmetry constraint was used for any

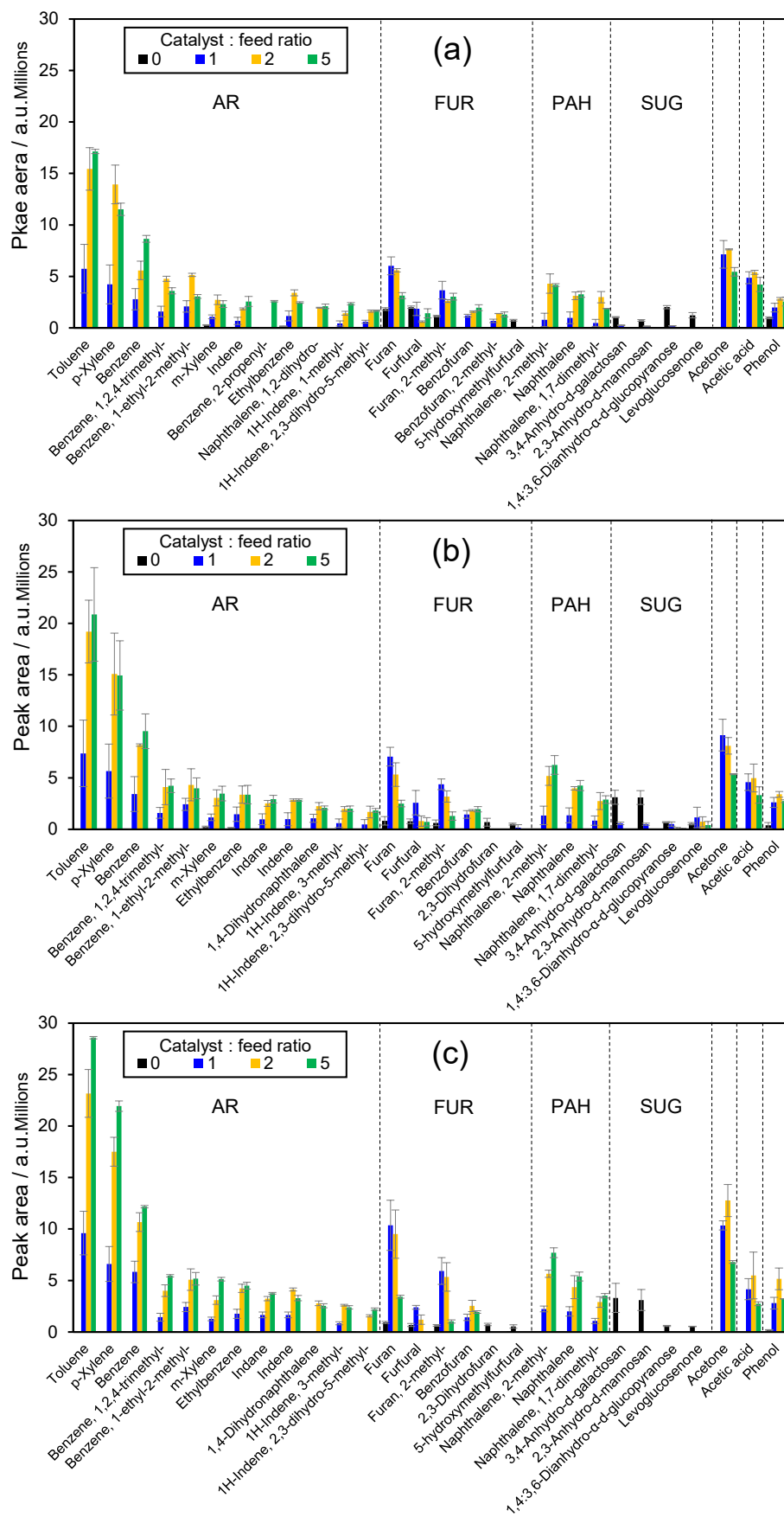


Fig. 2. Abundance of major identified products from LG thermal and catalytic fast pyrolysis at a) 500 °C, b) 550 °C, and c) 600 °C.

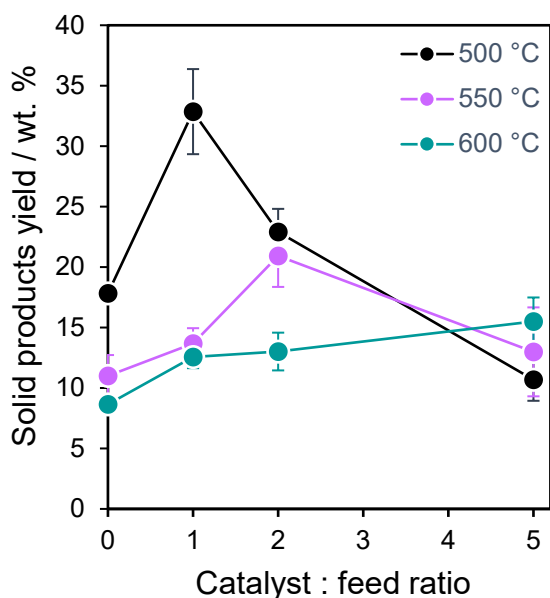


Fig. 3. Impact of temperature and catalyst: feed ratio on the formation of solid products in the thermal and catalytic pyrolysis of LG using HZSM-5 as catalyst.

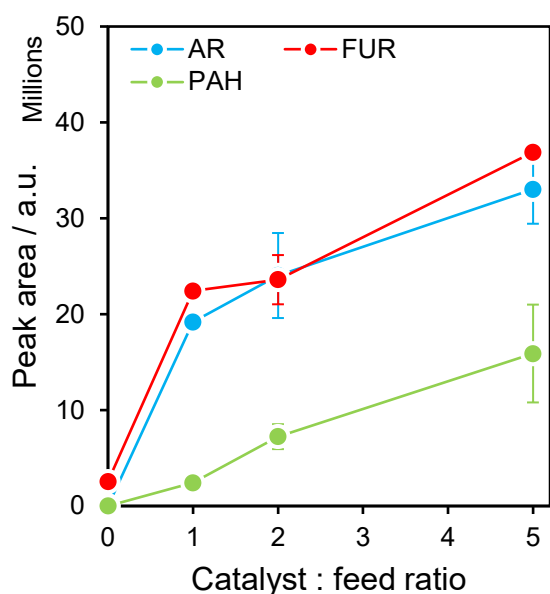


Fig. 4. Abundance of the main groups of products from the thermal and catalytic fast pyrolysis of furfural at 600 °C using HZSM-5 as catalyst.

modelling. The energy of the product was defined as the energy difference with the reactant. The transition state (TS) was completely determined by the LST/QST method, and the energy barriers of reactions (E_{barrier}) were determined by the difference between the energies of transition state and reactant, as shown in Eq. (2), where $E_{\text{transition state}}$ and E_{reactant} are the total energies of the transition state and reactant of a reaction, respectively.

$$E_{\text{barrier}} = E_{\text{transition state}} - E_{\text{reactant}} \quad (2)$$

3. Results and discussion

3.1. Levoglucosan pyrolysis

As demonstrated in Fig. 1, the products of LG thermal and catalytic

fast pyrolysis could be categorised into 4 major groups; anhydrosugars (SUG), furanic compounds (FUR), (mono)aromatic hydrocarbons (AR), and polyaromatic hydrocarbons (PAH). Non-catalytic fast pyrolysis (represented by a catalyst: feed ratio of 0) of LG mainly resulted in the formation of SUGs, such as anhydrogalactosan and anhydromannosan. FURs, including HMF and furfural, were detected as well, as shown in more detail in Fig. 2. The increase in the non-catalytic pyrolysis temperature resulted in an enhancement in the formation of all groups of products, however this impact is more pronounced for ARs, as illustrated in Fig. 1 and Fig. 2.

On the other hand, when HZSM-5 was present, regardless of the reaction temperature, no SUGs were detected, suggesting that they were readily converted over the catalyst. Furthermore, by increasing catalyst: feed ratio from 0 to 1, the concentration of FURs increased substantially, indicating that HZSM-5 catalysed their formation via the decomposition of LG and/or the conversion of the primary pyrolysis products of LG. However, a further increase in catalyst: feed ratio led to a decrease in furanic content. This is also evident from Fig. 2, in which the abundance of furan, furfural and 2-methylfuran goes through a maximum with increasing catalyst: feed ratio, suggesting that FURs are an intermediate product of the catalytic conversion of LG and that HZSM-5 further facilitates their conversion to ARs, either through a cracking step followed by aromatisation of acyclic fragments [55], or via Diel-Alder condensation of furan and olefins followed by dehydration to form aromatic products [56], or a combination of the above.

Moreover, as presented in Fig. 2, the formation of acetic acid was observed during catalytic fast pyrolysis of LG over HZSM-5, in agreement with the literature [57,58]. Analogous to FURs, the abundance of acetic acid as a function of catalyst: feed ratio reached a maximum when equal amounts of catalyst and feed were used. This indicated that acetic acid was also an intermediate product of the catalytic conversion of LG. Moreover, the formation of significant amounts of acetone was observed, which also went through a maximum at catalyst: feed = 2. The above can be explained in terms of HZSM-5-catalysed formation of acetic acid from LG, followed by ketonisation of acetic acid towards acetone. Fig. 1 and Fig. 2 also show that the abundance of ARs, mainly benzene, toluene and xylene (BTX) increased progressively with an increasing catalyst: feed ratio from 0 to 2, however this increasing trend slows down for a catalyst: feed ratio higher than 2, owing to the polymerisation of monoaromatics and formation of PAH molecules such as naphthalene and 2-methylnaphthalene. The details of identified products from LG thermal and catalytic pyrolysis are presented in Table S1-S12.

Furthermore, to explore solid residue formation during LG catalytic fast pyrolysis in the presence of HZSM-5, the sample tube weights were measured pre- and post-combustion. As Fig. 3 demonstrates, reaction temperature and catalyst: feed ratio had a significant influence on the solid residue yield. It has been previously reported that during thermal pyrolysis, LG can get polymerised into polysaccharides, and subsequently get carbonised to form char [59]. LG can also get degraded to low molecular weight (LMW) products [33], which can undergo tandem reactions over a heterogeneous catalyst such as HZSM-5 to form PAHs that get trapped in the catalyst pores and form coke [55]. Fig. 3 shows that during the thermal pyrolysis of LG (catalyst: feed ratio = 0), the solid product yield (char) dropped from 17.8 % at 500 °C to 8.6 % at 600 °C. This significant reduction in char yield with increasing pyrolysis temperature indicated that the polymerisation of LG vapours and its anhydrous derivatives were less energy intensive than their decomposition to LMW products. At 500 °C, the solid product yield reached a maximum of 32.9 % at catalyst: feed ratio = 1, attributable to carbonaceous residue formation via both mechanisms (char formation as well as coke deposition on the catalyst). Increasing the pyrolysis temperature shifted the maximum carbon yield to higher catalyst: feed ratios, suggesting a switchover from char formation mechanism to coke formation mechanism. In other words, as the catalyst: feed ratio increased, the catalytic routes that led to coke formation became dominant over the

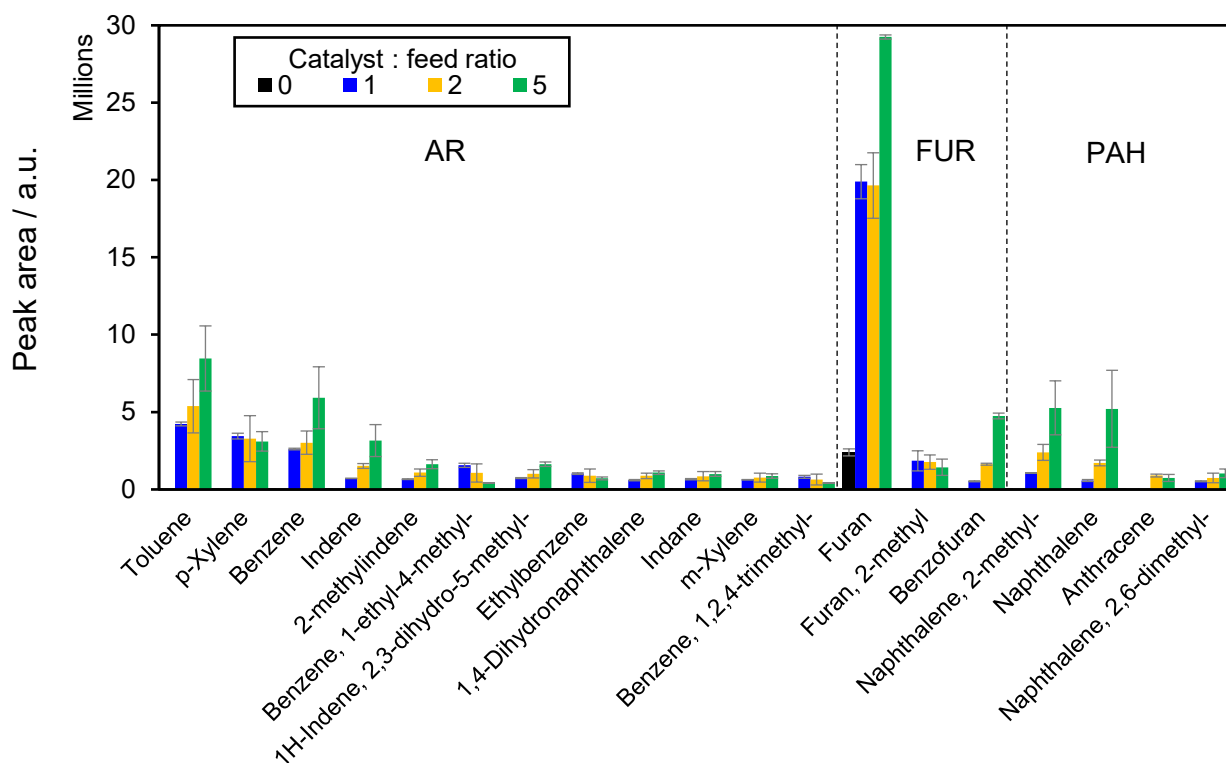


Fig. 5. Abundance of major identified products from furfural thermal and catalytic fast pyrolysis at 600 °C using HZSM-5 as catalyst.

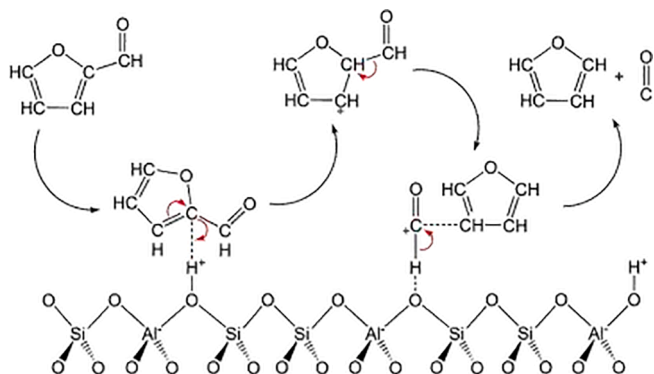


Fig. 6. Mechanism of furfural conversion to furan through decarbonylation over HZSM-5 [64].

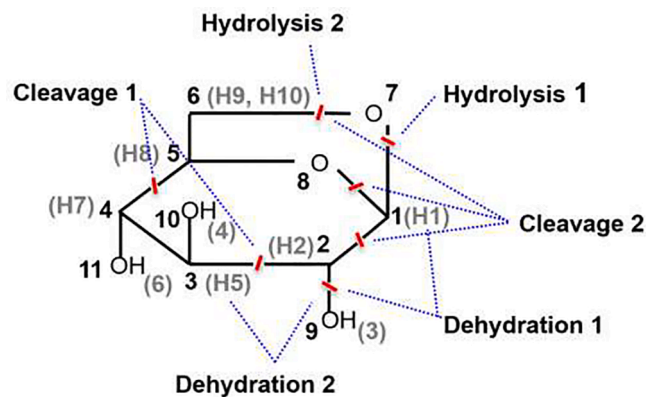


Fig. 7. Possible cleavages for the first step decomposition of LG.

char formation routes.

3.2. Intermediate: Furfural or furan?

To verify the hypothesis that FURs are the intermediate products of LG catalytic fast pyrolysis, thermal and catalytic pyrolysis of furfural was carried out, as a representative of FURs because it was among the major furanic products of LG catalytic fast pyrolysis. Other FURs, such as furan and 2-methylfuran were more prominent in the pyrolysis products of LG, however furfural was the only one that could be weighed with accuracy, owing to its relatively higher boiling point. In the absence of HZSM-5 and at 600 °C, furfural thermal fast pyrolysis did not yield many products, suggesting that the conversion of furfural requires a high activation energy. The only major identified product was furan with a relatively small peak area (Fig. 4). Also, a large furfural peak area was observed, indicating low furfural conversion. However, in the presence of HZSM-5, the conversion was enhanced and significant amounts of FURs, ARs and PAHs was observed in the product stream. Increasing the amount of catalyst resulted in a linear increase in the FUR, AR and PAH yield, as demonstrated in Fig. 4. Furan was by far the most significant furanic product observed, along with some 2-methylfuran and benzofuran (Fig. 5). Moreover, BTX accounted for the majority of the aromatics, while naphthalene and 2-methyl naphthalene were the most abundant PAHs (Fig. 5). These observations are in good agreement with the literature [19]. The details of identified products from furfural thermal and catalytic pyrolysis are presented in Table S13-S16.

Furfural can be converted into furan through decarbonylation (losing a CO molecule). Furfural decarbonylation is often catalysed by metal catalysts such as Pd at mild conditions ($T < 250$ °C) [60–63]. Alternatively, it can be catalysed by an acid catalyst like HZSM-5 [19,64]. In such a reaction, as illustrated in Fig. 6, the furfural molecule is initially adsorbed on the HZSM-5 surface. Then, the α -carbon is protonated by a Brønsted acid site and an intermediate arenium ion is formed. Subsequently, the positive charge is transferred to the β -carbon. In the next step, furan is formed via the decarbonylation transition state; the proton

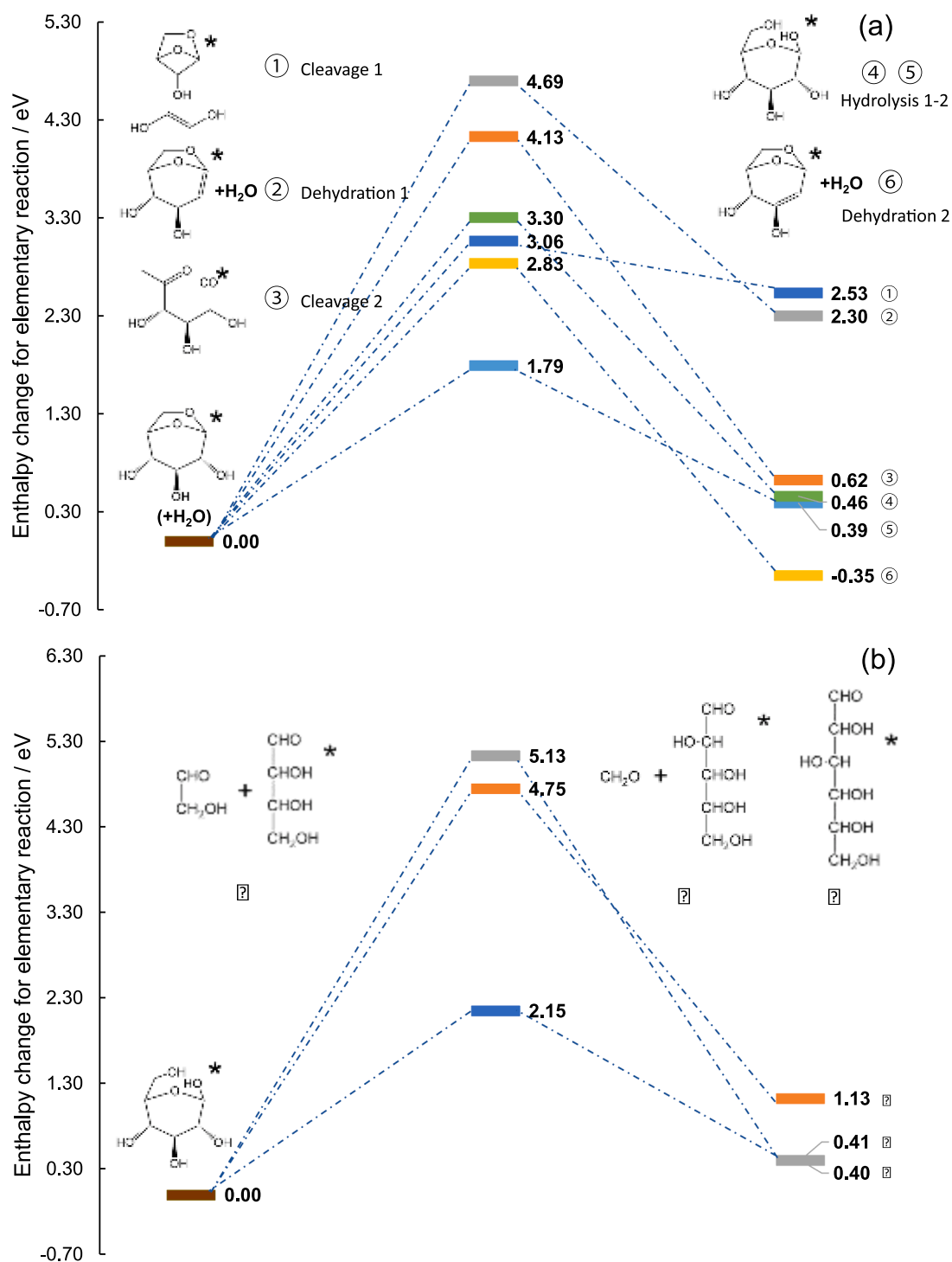


Fig. 8. Elementary reactions of the decomposition of (a) LG, (b) glucose (c) hexose chain (d) d-erythrose (e) erythrofuranose (star indicates the adsorbed compound over the Brønsted acid site).

is back-transferred to the oxygen of zeolite framework and at the same time the C—C bond is broken. Finally, furan and CO are desorbed from the HZSM-5 surface and the Brønsted acid site is regenerated.

The impact of catalyst: feed ratio on the solid product yields from the thermal and catalytic fast pyrolysis of furfural was investigated as well. Fig. S3 shows that thermal fast pyrolysis of furfural resulted in 1.3 % char yield. The relatively low char yield was consistent with low furfural conversion in the absence of a catalyst. However, in the presence of

HZSM-5, the solid product yield increased linearly as a function of catalyst: feed ratio, reaching 8.9 % at catalyst: feed = 5. This increase in the solid yield can be attributed to the formation of large molecules inside the pores of HZSM-5 and to char formation on the catalyst external surface as a result of condensation reactions.

In order to ensure there is no pathway from furan to furfural, thermal and catalyst pyrolysis of furan was carried out as well. As presented in Table S17 and Table S18, no furfural or its direct derivatives were

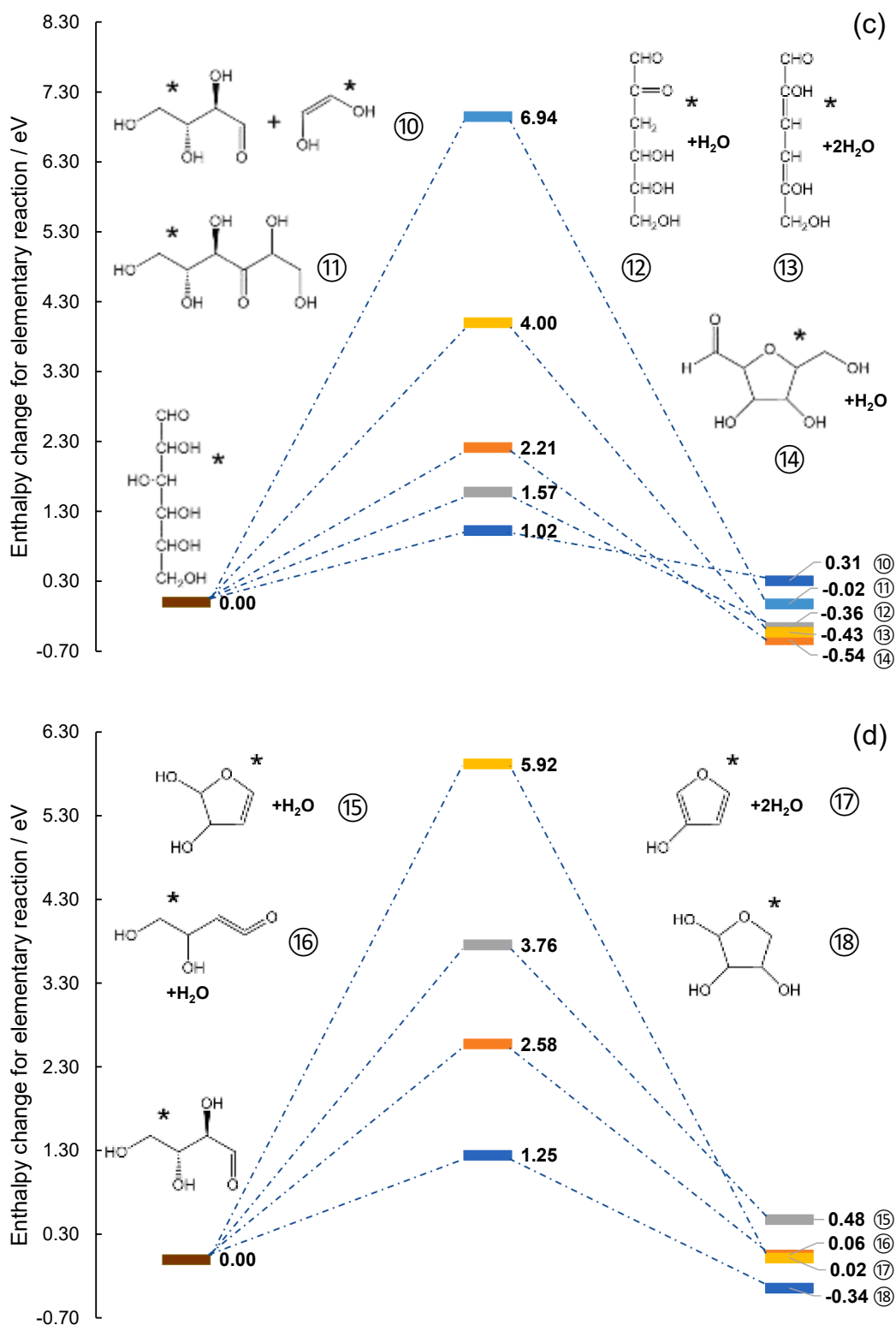


Fig. 8. (continued).

detected in either catalytic or non-catalytic pyrolysis products. While the majority of the products of furan thermal pyrolysis could not be identified, furan fast pyrolysis over HZSM-5 resulted mainly in the formation of benzofuran and 2-methyl benzofuran, as well as aromatic hydrocarbons such as BTX, indane, indene, and some PAHs including naphthalene. These results were in good agreement with the proposed furan pyrolysis mechanism over HZSM-5 in the literature that two furan

molecules can react with each other and lose an H₂O molecule to form benzofuran, which in turn can be cracked on the zeolite surface to form benzene and coke [56,65]. Furan, via decarbonylation, can get converted to propadiene which is subsequently transformed into olefins via oligomerisation and cracking. The olefins can then react with each other on the HZSM-5 surface to form single-ring aromatics. The presence of furan, various olefins and aromatic hydrocarbons creates a mixture that

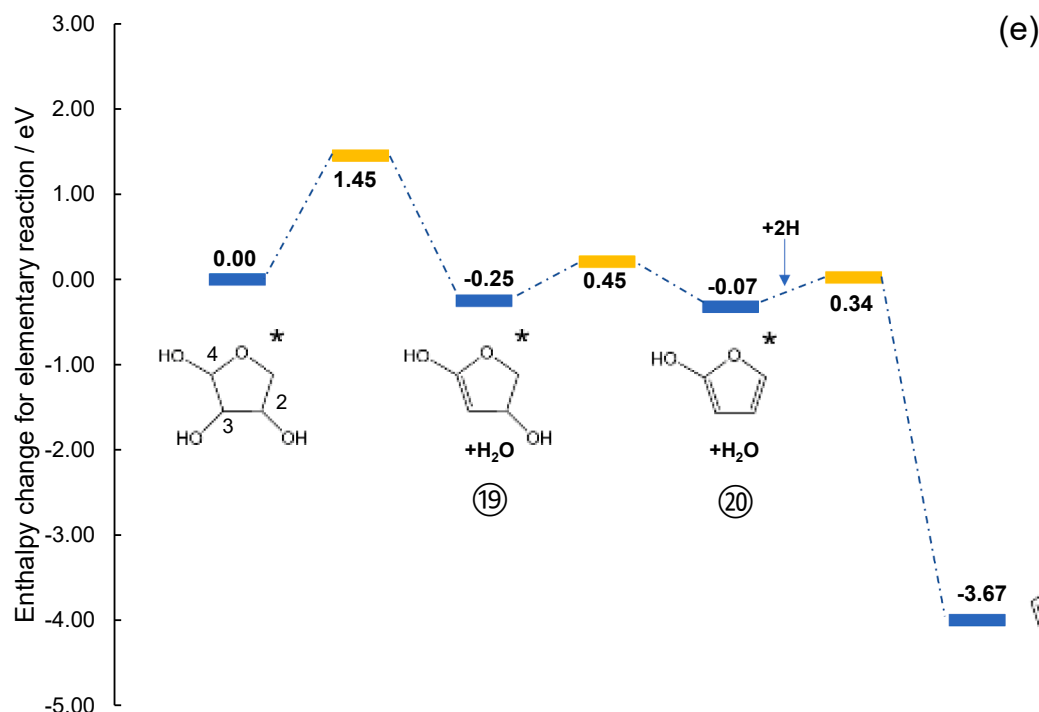


Fig. 8. (continued).

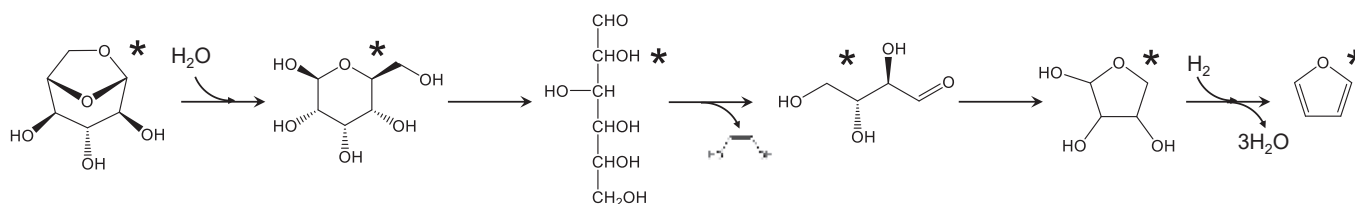


Fig. 9. Alternative catalytic conversion pathways of LG to furan over HZSM-5.

is known as a ‘hydrocarbon pool’ [66]. The hydrocarbon pool products can react together to form aromatic hydrocarbons with alkyl branches, indenenes, PAHs and eventually coke. The olefins will join the hydrocarbon pool and continue reacting as explained before. Another potential transformation route for furan is via hydrolysis which results in the production of olefins and CO_2 [65].

3.3. DFT confirmation of levoglucosan-to-furan route

To reveal the underlying mechanism for the decomposition of LG, the reaction pathways over Brønsted acid site were thoroughly analysed through DFT modelling, and the details of the elementary catalytic reactions (including structures of reactant, transition state and product) are presented in Table S19. Six possible scenarios were considered for the initial decomposition of LG, as shown in Fig. 7 [33]. Specifically, the cracking pathway (Cleavage 1) consists of the cleavages of C(2)–C(3) and C(4)–C(5) bonds. Another cracking pathway (Cleavage 2) includes cleavages of C(1)–O(7), C(1)–O(8) and C(1)–C(2). The dehydration reaction was predicted to take place via the cracking of C(2)–OH bond with adjacent hydrogen atoms of H(1) or H(5). This is because the O(9) that is connected to C(2) is found to be the most reactive oxygen atom for the electrophilic attack to the Brønsted acid site of HZSM-5 (Fig. S4). For all the above reactions, the energy barriers and reaction energies were determined by DFT modelling, as shown in Fig. 8a.

The modelling results predicted that at the beginning of LG decomposition over Brønsted acid sites, the catalytic cracking of C–C (Cleavage 1 in Fig. 7) had an energy barrier of 3.06 eV, and the C–O

cracking (Cleavage 2 in Fig. 7) had an energy barrier of 4.13 eV. Both of them are higher compared to non-catalytic scenario [33]. Regarding dehydration reactions, the dehydration of O(9)H(3) and H(5) showed a lower energy barrier of 2.83 eV, compared to the other dehydration reaction of O(9)H(3) and H(1), which had an energy barrier of 4.69 eV. Among the above reactions, it was found that the dehydration reaction (⑥), which is the only exothermic reaction, is the most favourable route over HZSM-5. Since LG decomposition is more prone to dehydration, H_2O is expected to be present in the fast pyrolysis vapours. Therefore, H_2O will be available to react with LG and for this reason hydrolysis reactions of LG were also considered as the first step in this study. The hydrolysis of LG may take place to either bond C(1)–C(7) (④) or bond C(6)–C(7) (⑤), as shown in Fig. 8a [25]. Both hydrolysis reactions are endothermic and lead to the formation of the same product, glucose, however, they have different energy barriers of 1.79 eV and 3.30 eV, respectively. Besides, it is noted that the hydrolysis reaction (③) gives rise to the lowest energy barrier for the initial decomposition of LG, indicating glucose would become an intermediate for the subsequent reactions [25], however glucose is unstable at high temperatures, and this may result in its absence in the products observed in our experiments.

Following the hydrolysis of LG, three reactions were considered to take place during the decomposition of glucose, including two cracking reactions and one ring opening reaction (Fig. 8b). The results indicate that glucose may get cracked with an energy barrier of 4.75 eV (⑦) to produce a C_4 compound and glycolaldehyde ($\text{C}_2\text{H}_4\text{O}_2$), which is commonly seen in cellulose fast pyrolysis [24,25]. However, in this work

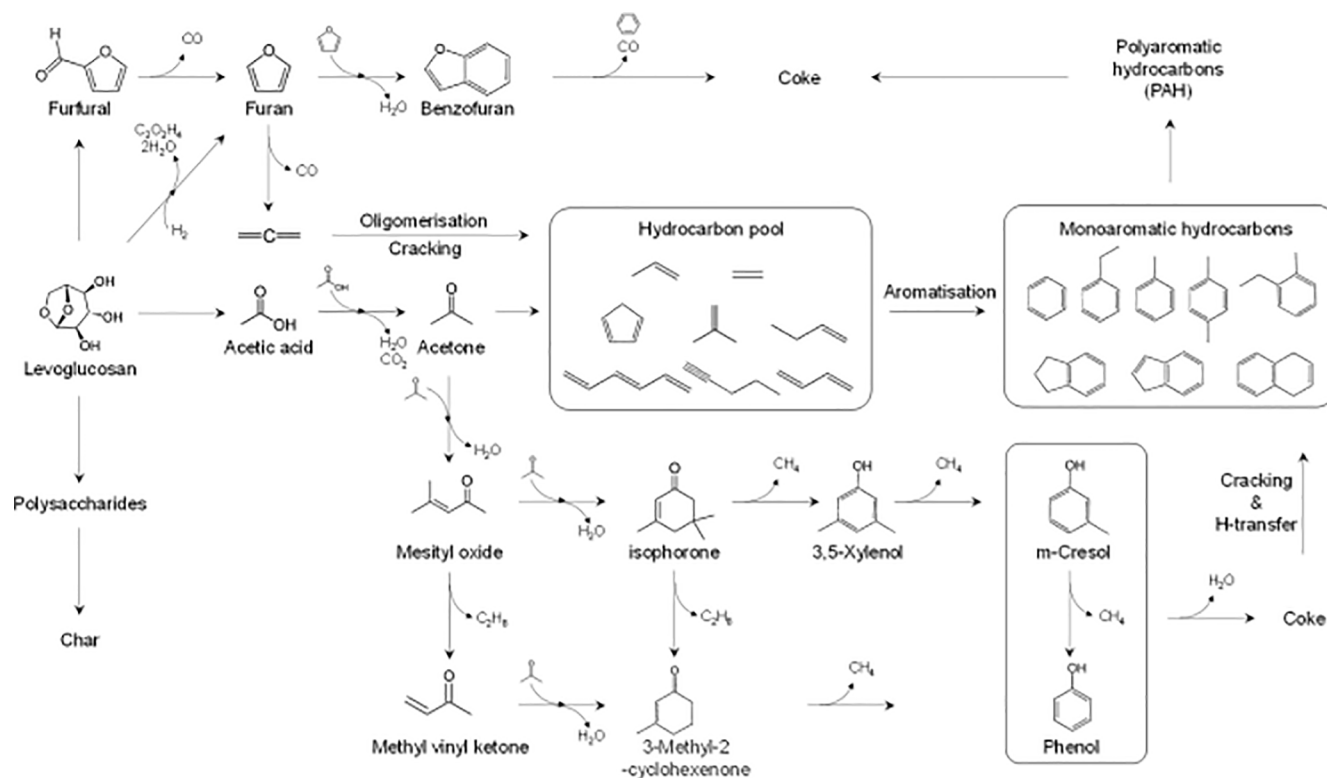


Fig. 10. Proposed reaction network for the catalytic conversion of LG over HZSM-5.

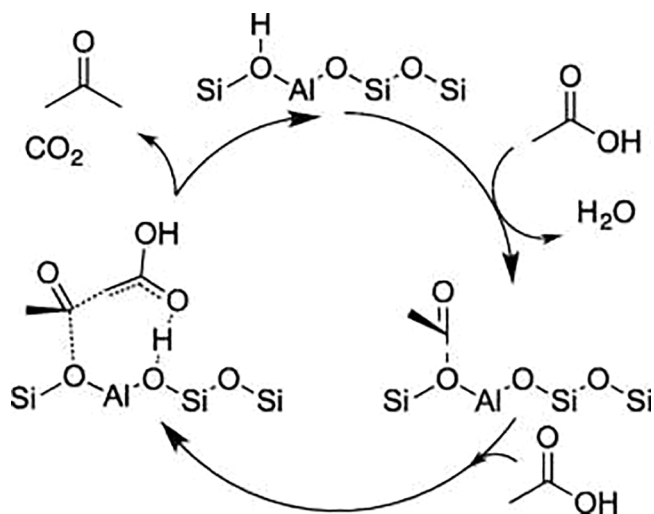


Fig. 11. Reaction mechanism for ketonisation of acetic acid over acidic zeolite. Reprinted from reference [70] with permission from Elsevier.

glycolaldehyde was not detected in the LG pyrolysis products as its MS fingerprints (m/z 29, 31 and 32) were not within the m/z range of the MS. Glucose can also undergo another cracking route to produce formaldehyde and a C_5 compound (Ⓒ), although this pathway seems to be more difficult with an energy barrier of 5.13 eV. The most facile decomposition pathway for glucose is found to be the ring opening reaction with an energy barrier of 2.15 eV (Ⓓ), leading to the formation of a linear C_6 compound (hexose), as shown in Fig. 8b. This is in line with the reported mechanism in the non-catalytic scenario [25].

Once the linear hexose intermediate was produced, there were a variety of sequential cracking pathways [25,34], as shown in Fig. 8c. The hexose chain is likely to undergo dehydration reactions with two

different pathways, producing anhydrosugars (Ⓔ) and (Ⓕ). One of them is produced by two simultaneous dehydrations with a relatively high energy barrier of 4.00 eV, and the other dehydration leading to the carbonyl formation with a low energy barrier of 1.57 eV. These compounds can be precursors of HMF before further cyclisation and dehydrations. Besides, HMF is also possibly produced from 2,5-anhydrohexose through direct dehydration, the latter compound results from the direct cyclisation of the hexose chain, with a formation energy barrier of 2.21 eV over a Brønsted acid site (Ⓓ). HMF is a common component in bio-crude, and would lead to the formation of furanics over Brønsted acid sites [25,67,68]. Apart from the HMF pathway, the linear C_6 molecule is also predicted to undergo direct cracking to produce a C_4 compound (d-erythrose) and an unstable 1,2-ethenediol (Ⓗ). 1,2-Ethenediol is likely to get isomerised to glycolaldehyde, which is deemed as the main source of glycolaldehyde during LG decomposition. Although this reaction is slightly endothermic with a reaction enthalpy of 0.31 eV, it is facilitated by Brønsted acid sites with a small energy barrier of 1.02 eV. This low energy barrier indicates that this reaction is preferable over the HMF pathway.

In addition, the modelling indicates that the hexose chain is unlikely to be isomerised over the Brønsted acid sites, as shown in Fig. 8c (Ⓙ). Therefore, the reaction in this step is most likely to produce a C_4 compound (d-erythrose) and a C_2 compound (glycolaldehyde) as the products. This reaction pathway was also found to be preferable in the free-molecule decomposition [34], but it is further facilitated by the Brønsted acid site through decreasing the energy barrier by 0.73 eV.

d-Erythrose would then undergo four different reactions, including cyclisation and dehydration, as illustrated in Fig. 8d. The DFT modelling results predicted that the simultaneous cyclisation and dehydration reactions (Ⓜ and Ⓨ) may have extremely high energy barriers of 3.76 eV and 5.92 eV, respectively, whereas sole dehydration reaction had a lower energy barrier of 2.58 eV (Ⓩ). Furthermore, an energy barrier as low as 1.25 eV was observed for the reaction of sole cyclisation (Ⓛ), indicating it is more likely to take place in this step, to produce erythrorufanose, which would be a precursor for furanic compounds. This is

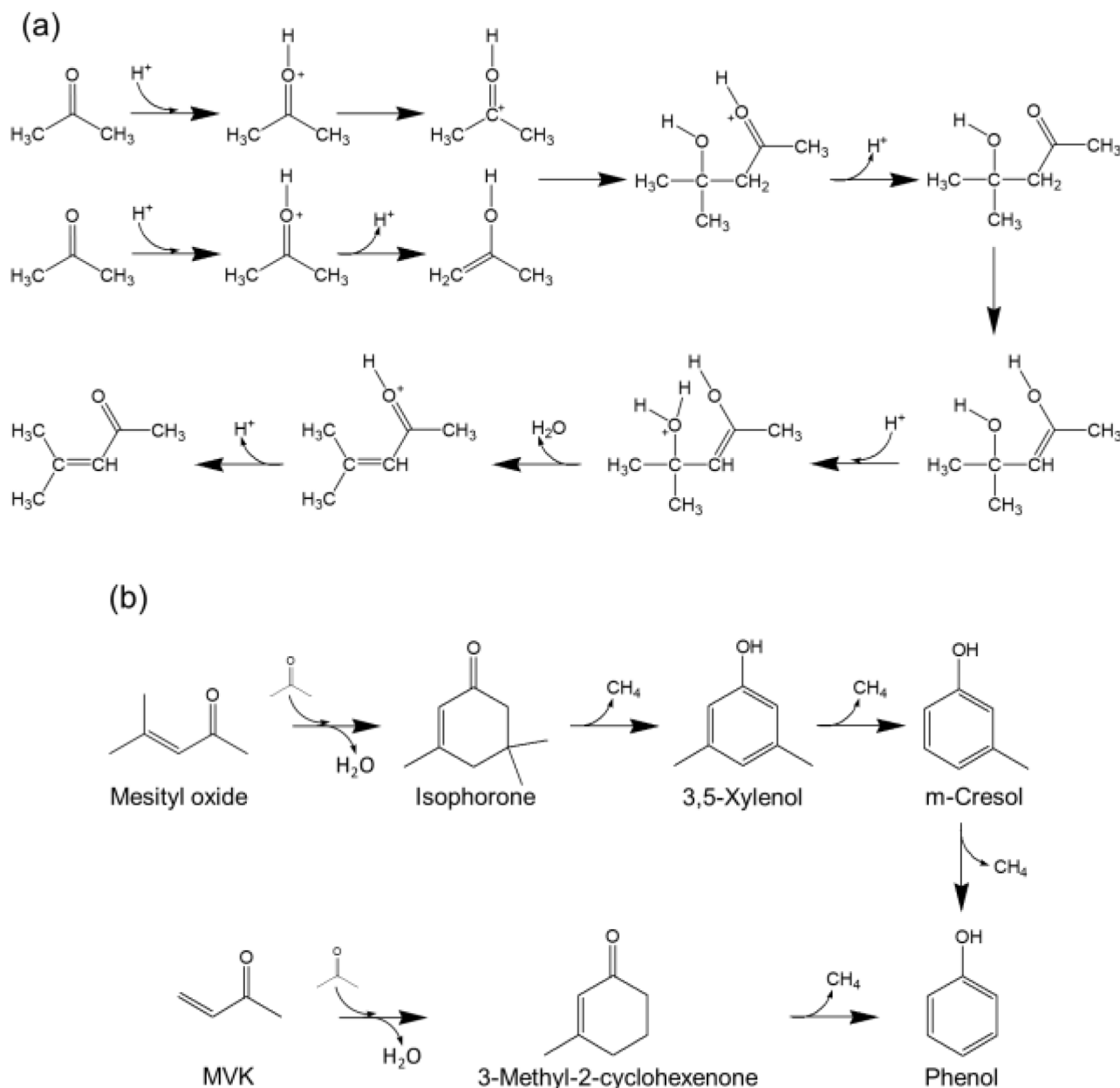


Fig. 12. a) Brønsted acid catalyzed aldol condensation reaction mechanism, b) Proposed reaction pathways from mesityl oxide and methyl vinyl ketone (MKV) to phenolic compounds.

in line with a previous study in free molecule scenario that the cyclisation of the C_4 compound is the most favourable pathway [34]. Our model also predicts that the energy barrier of this reaction is lowered by 0.82 eV in the presence of a Brønsted acid site, which further facilitates the decomposition of this key intermediate of LG.

A series of dehydration reactions of erythrofuranose were then modelled, and the most kinetically favourable pathway is shown in Fig. 8e. The results indicate that the hydroxyl group on C(3) would most likely crack with the H linked to C(2), leading to the first exothermic dehydration with an energy barrier of 1.45 eV. This energy barrier is found to be 1.67 eV lower than that of predicted for the dehydration pathway of erythrofuranose in a free molecule reaction, where the hydroxyl group on C(2) cracks with the H on C(3) was found to be the most preferable reaction [34]. This step would be followed by another dehydration of hydroxyl (on C(4)) and adjacent H to produce 2-hydroxyfuran with a small energy barrier of 0.45 eV. As the obtained 2-hydroxyfuran can hardly undergo any intramolecular dehydrations,

hydrogenolysis with the hydrogen that exists in the reaction medium from condensation reactions can be an alternative option. The hydrogenolysis of 2-hydroxyfuran would directly lead to the production of furan. To model this step of the reaction, two separated H atoms were added beside 2-hydroxyfuran to eliminate the effect of H_2 dissociation, as shown in Fig. S5. The activation energy for this dehydroxylation step turns out to be as small as 0.34 eV and it results in substantial heat release (-3.67 eV). However, the energy barrier for the same reaction, but using molecular H_2 , will be much larger (3.43 eV), as shown in Fig. S6. This result suggests that the formation of furan would be remarkably facilitated by the presence of atomic H in surroundings. As the experiments in this study were carried out under inert environment, it is speculated that the H atoms generated during the formation of condensed hydrocarbons (e.g. alkenes) and coke on the catalysts are most likely to take part in the hydrogenolysis of 2-hydroxyfuran [66,69].

The overall reaction pathway from LG to furan established by our DFT modelling which agrees well with our experimental results is shown

in Fig. 9, demonstrating that FURs are key intermediates between LG and ARs.

3.4. Proposed overall reaction network

Based both on the experimental observations and the DFT calculations, a reaction network for the conversion of LG over HZSM-5, is presented in Fig. 10. In addition to the previously known LG → furfural → furan route, our DFT calculations show that there is a direct route (not through furfural) from LG to furan, consistent with our experimental results that showed significantly more furan formation from LG than furfural formation.

Acetic acid was also one of the major intermediate products of LG catalytic fast pyrolysis. The ketonisation of acetic acid over acidic metal oxides is likely to take place via formation of a surface acyl by dehydration and subsequent coupling with a second activated acid molecule to form acetone and CO₂, as shown in Fig. 11 [70].

Acetone, formed from acetic acid ketonisation, will then undergo aromatisation, with olefin hydrocarbons as intermediates [71,72]. Alternatively, two acetone molecules can react with each other through self-condensation to form mesityl oxide with diacetone alcohol as an intermediate [73–75], as demonstrated in the proposed reaction mechanism in Fig. 12a. Mesityl oxide in turn can go through cross aldol condensation with another acetone to produce isophorone, as shown in Fig. 12b [73,75]. Subsequently, isophorone can be cracked on HZSM-5 surface to yield phenolic compounds such as 3,5-xyleneol, m-cresol, and phenol. Another pathway from mesityl oxide to phenol is through cracking to form methyl vinyl ketone (MVK) followed by MVK cross aldol condensation with acetone (Fig. 12b). Table S1–S12 show that pyrolysis of LG in the presence of HZSM-5 resulted in considerably larger amounts of phenol than m-cresol, suggesting that either m-cresol is unstable under the reaction conditions, or the route from MKV to phenol is dominant.

The reaction mechanism for the downstream conversion of furans to ARs over Brønsted acid sites has been well established in the literature [66,76,77]. Essentially furan would undergo coupling reaction to produce benzofuran and coke, and the benzofuran would be then converted to ARs and CO at temperatures > 500 °C. Alternatively, furan would go through dehydration and Diels-Alder reaction at > 500 °C to produce ARs and olefin (ethylene and allene) directly. The olefins are known as a leaving group throughout the dehydration and decomposition of furan and are parts of the hydrocarbon pool [66]. It has also been widely reported that furan after alkylation (2-methylfuran and 2,5-dimethylfuran), would have higher selectivity to undergo dehydration and Diels-Alder condensations to produce ARs, especially xylene and toluene, because the side reaction of furan coupling is almost eliminated [56,78,79].

4. Conclusions

The reaction network for the catalytic fast pyrolysis of lignocellulosic biomass over a HZSM-5 catalyst was investigated experimentally and theoretically. Fast pyrolysis of LG, furfural and furan in the presence and absence of HZSM-5 was performed using Py-GC–MS–FID. LG was chosen as the primary decomposition product of cellulose, while furfural and furan were chosen as they were shown to be products of the catalytic and non-catalytic conversion of LG. The experimental results showed that in the absence of a catalyst, anhydrosugars, furan and furfural are the main products from the decomposition of LG. In the presence of HZSM-5, the amounts of furanic compounds, mono and polyaromatic hydrocarbons as well as acids and phenols in the product stream were increased significantly. The increase in the amount of catalyst led to a substantial increase in the amount of mono- and polyaromatic hydrocarbons at the expense of furanics, indicating that furanics are the key intermediate to aromatics. Catalytic fast pyrolysis of furfural further confirmed this hypothesis, revealing that mono- and polyaromatic hydrocarbons were

the main products when using furfural as starting material. The catalytic fast pyrolysis of furan revealed that there is no pathway from furan to furfural, however, still there is a route to aromatics with benzofuran as an intermediate. The higher abundance of furan compared to furfural suggested the possibility of an alternative route for the conversion of LG to furan without furfural as an intermediate. The mechanism of levoglucosan decomposition over Brønsted acid sites of HZSM-5 was further investigated by DFT modelling, and a plausible reaction pathway was established that supported the existence of a direct route from levoglucosan to furan without furfural as an intermediate via a series of sequential hydrolysis, ring-opening, cracking, cyclisation, and dehydration reactions with an energy barrier along the favourable pathway of 2.15 eV.

CRedit authorship contribution statement

Amin Osatiashtiani: Methodology, Investigation, Writing – original draft, Writing – review & editing. **Jiajun Zhang:** Methodology, Investigation, Writing – original draft, Writing – review & editing. **Stylianos D. Stefanidis:** Writing – original draft, Writing – review & editing. **Xiaolei Zhang:** Conceptualization, Funding acquisition, Supervision, Writing – review & editing. **Anthony V. Bridgwater:** Conceptualization, Funding acquisition, Supervision, Writing – review & editing.

Declaration of Competing Interest

The authors declare that they have no known competing financial interests or personal relationships that could have appeared to influence the work reported in this paper.

Acknowledgement

The authors would like to acknowledge financial support from the Leverhulme Trust Research Grant (RPG-2017-254) and support from EPSRC First Grant (EP/R010986/1). The authors are also grateful for computational support from the UK Materials and Molecular Modelling Hub, which is partially funded by EPSRC (EP/P020194), for which access was obtained via the UKCP consortium and funded by EPSRC grant ref EP/P022561/1.

Appendix A. Supplementary data

Supplementary data to this article can be found online at <https://doi.org/10.1016/j.fuel.2022.125279>.

References

- [1] International Energy Agency, Renewables 2018, Paris, 2018.
- [2] Carlson TR, Vispute TP, Huber GW. *ChemSusChem* 2008;1:397–400.
- [3] Mohan D, Pittman CU, Steele PH. *Energy Fuels* 2006;20:848–89.
- [4] Mullen CA, Boateng AA. *Energy Fuels* 2008;22:2104–9.
- [5] Banks SW, Nowakowski DJ, Bridgwater AV. *Energy Fuels* 2016;30:8009–18.
- [6] Feroso J, Pizarro P, Coronado JM, Serrano DP. *WIREs Energy Environ* 2017;6:e245.
- [7] Carlson TR, Cheng Y-T, Jae J, Huber GW. *Energy Environ Sci* 2011;4:145–61.
- [8] Succi J, Saraeian A, Stefanidis SD, Banks SW, Shanks BH, Bridgwater T. *J Anal Appl Pyrolysis* 2019;104710.
- [9] Hoff TC, Gardner DW, Thilakarathne R, Proano-Aviles J, Brown RC, Tessonier J-P. *Appl Catal A Gen* 2017;529:68–78.
- [10] Du X, Ma X, Li Y, Chen P, Liu Y, Lin X, et al. *Bioresour Technol* 2013;139:397–401.
- [11] Jae J, Tompsett GA, Foster AJ, Hammond KD, Auerbach SM, Lobo RF, et al. *J Catal* 2011;279:257–68.
- [12] Liu C, Wang H, Karim AM, Sun J, Wang Y. *Chem Soc Rev* 2014;43:7594–623.
- [13] Stefanidis SD, Kalogiannis KG, Lappas AA. *WIREs Energy Environ* 2018;7:e281.
- [14] Talmadge MS, Baldwin RM, Biddy MJ, McCormick RL, Beckham GT, Ferguson GA, et al. *Green Chem* 2014;16:407–53.
- [15] Yang H, Coolman R, Karanjkar P, Wang H, Dornath P, Chen H, et al. *Green Chem* 2017;19:286–97.
- [16] Yang X, Fu Z, Han D, Zhao Y, Li R, Wu Y. *Renew Energy* 2020;147:1120–30.
- [17] Hemberger P, Custodis VBF, Bodi A, Gerber T, van Bokhoven JA. *Nat Commun* 2017;8:15946.
- [18] Carlson TR, Jae J, Lin Y-C, Tompsett GA, Huber GW. *J Catal* 2010;270:110–24.

- [19] Fanchiang W-L, Lin Y-C. *Appl Catal A Gen* 2012;419–420:102–10.
- [20] Uemura K, Appari S, Kudo S, Hayashi J, Einaga H, Norinaga K. *Fuel Process Technol* 2015;136:73–8.
- [21] Yan K, Li H. *Energy Fuels* 2021;35:45–62.
- [22] Lu Q, Yang X, Dong C, Zhang Z, Zhang X, Zhu X. *J Anal Appl Pyrolysis* 2011;92:430–8.
- [23] Ye X, Lu Q, Jiang X, Wang X, Hu B, Li W, et al. *J Therm Anal Calorim* 2017;1–10.
- [24] Piskorz J, Radlein D, Scott DS. *J Anal Appl Pyrolysis* 1986;9:121–37.
- [25] Shen DK, Gu S. *Bioresour Technol* 2009;100:6496–504.
- [26] Evans RJ, Milne TA. *Energy Fuels* 1987;1:123–37.
- [27] Shaw A, Zhang X, Kaban L, Li J. *Fuel* 2021;286:119444.
- [28] Zhang X, Yang W, Dong C. *J Anal Appl Pyrolysis* 2013;104:19–27.
- [29] Lin Y-C, Cho J, Tompsett GA, Westmoreland PR, Huber GW. *J Phys Chem C* 2009;113:20097–107.
- [30] Maliekkal V, Maduskar S, Saxon DJ, Nasiri M, Reineke TM, Neurock M, et al. *ACS Catal* 2019;9:1943–55.
- [31] Maduskar S, Maliekkal V, Neurock M, Dauenhauer PJ, Sustain ACS. *Chem Eng* 2018;6:7017–25.
- [32] Patwardhan PR, Satrio JA, Brown RC, Shanks BH. *J Anal Appl Pyrolysis* 2009;86:323–30.
- [33] Zhang X, Yang W, Blasiak W. *J Anal Appl Pyrolysis* 2012;96:110–9.
- [34] Fang Y, Li J, Chen Y, Lu Q, Yang H, Wang X, et al. *Energy Fuels* 2018;32:9519–29.
- [35] Seshadri V, Westmoreland PR. *J Phys Chem A* 2013;116(2012):11997–2001.
- [36] Seshadri V, Westmoreland PR. *Catal Today* 2016;269:110–21.
- [37] Mettler MS, Paulsen AD, Vlachos DG, Dauenhauer PJ. *Energy Environ Sci* 2012;5:7864–8.
- [38] Vinu R, Broadbelt LJ. *Energy Environ Sci* 2012;5:9808–26.
- [39] Bai X, Johnston P, Sadula S, Brown RC. *J Anal Appl Pyrolysis* 2013;99:58–65.
- [40] Bai X, Johnston P, Brown RC. *J Anal Appl Pyrolysis* 2013;99:130–6.
- [41] Bai X, Brown RC. *J Anal Appl Pyrolysis* 2014;105:363–8.
- [42] Zhou X, Nolte MW, Mayes HB, Shanks BH, Broadbelt LJ. *Ind Eng Chem Res* 2014;53:13274–89.
- [43] Zhou X, Nolte MW, Shanks BH, Broadbelt LJ. *Ind & Eng Chem Res* 2014;53:13290–301.
- [44] Mayes HB, Nolte MW, Beckham GT, Shanks BH, Broadbelt LJ, Sustain ACS. *Chem Eng* 2014;2:1461–73.
- [45] Zhang X, Yang W, Blasiak W. *Fuel* 2013;109:476–83.
- [46] Delley B. *J Chem Phys* 1990;92:508–17.
- [47] Segall MD, Lindan PJD, Probert MJ, Pickard CJ, Hasnip PJ, Clark SJ, et al. *J Phys Condens Matter* 2002;14:2717–44.
- [48] Perdew JP, Burke K, Ernzerhof M. *Phys Rev Lett* 1996;77:3865–8.
- [49] Grimme S. *J Comput Chem* 2006;27:1787–99.
- [50] Lejaeghere K, Van Speybroeck V, Van Oost G, Cottenier S. *Crit Rev Solid State Mater Sci* 2014;39:1–24.
- [51] Pickard CJ, Winkler B, Chen RK, Payne MC, Lee MH, Lin JS, et al. *Phys Rev Lett* 2000;85:5122–5.
- [52] Zhang J, Zhang X, Osatiashtiani A, Luo KH, Shen D, Li J, et al. *Mol Catal* 2021;499:111289.
- [53] Huang Y, Dong X, Li M, Yu Y, Gao J, Zheng Y, et al. *Catal Sci Technol* 2015;5:1093–105.
- [54] Huang Y, Dong X, Li M, Zhang M, Yu Y. *RSC Adv* 2014;4:14573–81.
- [55] Du S, Gamliel DP, Giotto MV, Valla JA, Bollas GM. *Appl Catal A Gen* 2016;513:67–81.
- [56] Cheng Y-T, Huber GW. *Green Chem* 2012;14:3114–25.
- [57] Lu Q, Wu Y, Hu B, Liu J, Liu D, Dong C, et al. *Cellulose* 2019;26:8279–90.
- [58] Hosoya T, Kawamoto H, Saka S. *J Anal Appl Pyrolysis* 2008;83:64–70.
- [59] Kawamoto H, Murayama M, Saka S. *J Wood Sci* 2003;49:469–73.
- [60] Ishida T, Kume K, Kinjo K, Honma T, Nakada K, Ohashi H, et al. *ChemSusChem* 2016;9:3441–7.
- [61] Zhang W, Zhu Y, Niu S, Li Y. *J Mol Catal A Chem* 2011;335:71–81.
- [62] Mitra J, Zhou X, Rauchfuss T. *Green Chem* 2015;17:307–13.
- [63] Modak A, Deb A, Patra T, Rana S, Maity S, Maiti D. *Chem Commun* 2012;48:4253–5.
- [64] Charoenwiangnuea P, Maihom T, Kongpracha P, Sirijaraensre J, Limtrakul J. *RSC Adv* 2016;6:105888–94.
- [65] Gilbert CJ, Espindola JS, Conner Jr WC, Trierweiler JO, Huber GW. *ChemCatChem* 2014;6:2497–500.
- [66] Cheng YT, Huber GW. *ACS Catal* 2011;1:611–28.
- [67] Wang K, Zhang J, Shanks BH, Brown RC. *Green Chem* 2015;17:557–64.
- [68] Kåldström M, Kumar N, Heikkilä T, Tiitta M, Salmi T, Murzin DY. *ChemCatChem* 2010;2:539–46.
- [69] Zhang J, Fidalgo B, Kolios A, Shen D, Gu S. *Chem Eng J* 2018;336:211–22.
- [70] Gumidyala A, Sooknoi T, Crossley S. *J Catal* 2016;340:76–84.
- [71] Jahangiri H, Osatiashtiani A, Ouadi M, Hornung A, Lee AF, Wilson K. *Catalysts* 2019;9:841.
- [72] Gayubo AG, Aguayo AT, Atutxa A, Aguado R, Olazar M, Bilbao J. *Ind Eng Chem Res* 2004;43:2619–26.
- [73] Sun J, Baylon RAL, Liu C, Mei D, Martin KJ, Venkitasubramanian P, et al. *J Am Chem Soc* 2016;138:507–17.
- [74] Baylon RAL, Sun J, Martin KJ, Venkitasubramanian P, Wang Y. *Chem Commun* 2016;52:4975–8.
- [75] Ramanamurthy KV, Salvapati GS, Indian J. Chem - Sect B Org Med Chem 1999;38:24–8.
- [76] Teixeira IVOF. *Catalytic Conversion of Biomass-Derived Platform Molecules Over Zeolites Catalytic Conversion of Biomass-Derived Platform Molecules Over Zeolites*. University of Oxford; 2017.
- [77] Cheng YT, Jae J, Shi J, Fan W, Huber GW. *Angew Chemie-International Ed* 2012;51:1387–90.
- [78] Williams CL, Chang C-C, Do P, Nikbin N, Caratzoulas S, Vlachos DG, et al. *ACS Catal* 2012;2:935–9.
- [79] Wang D, Omsundsen CM, Taarning E, Dumesic JA. *ChemCatChem* 2013;5:2044–50.